Breakdown of classical electrostatics in the depolarization of quantum wires and nanotubes

L. Shan and E. G. Mishchenko

Phys. Rev. B **96**, 195441 — Published 30 November 2017

DOI: 10.1103/PhysRevB.96.195441

Breakdown of classical electrostatics in the depolarization of quantum wires and nanotubes

L. Shan and E. G. Mishchenko
Department of Physics and Astronomy, University of Utah, Salt Lake City, Utah 84112, USA

In quantum wires, such as metallic nanotubes, the optical absorption of the transverse polarization is controlled by the depolarization effect which stems from the redistribution of conduction electrons around the circumference of the system. The traditional electrostatics treatment of the depolarization effect relies on approximating the system by a cylinder with some effective dielectric permittivity. We demonstrate that this simple intuitive picture does not adequately describe optical absorption near its threshold, as the depolarization effect becomes dominated by many-body correlations which strongly modify the spectral dependence of absorption.

PACS numbers: 73.21.Hb, 73.22.-f

Introduction. Quantum wires have a limited number of conducting channels N, which originate from confinement of electrons in the transverse direction [1]. Transitions between such channels determine the response of a wire to a transverse electric field. For example, in the case of a carbon nanotube [2], or similarly rolled two-dimensional hexagonal crystals, such as tungsten sulfate and gallium nitride nanotubes, the transverse polarization induced by the electric field arises from the motion of carriers around the circumference of the nanotube. In the quantum picture, this motion amounts to a redistribution of electrons between different subbands corresponding to different values of the azimuthal angular momentum m. According to the band structure of metallic carbon nanotubes, see Fig. 1, the subbands with $m \neq 0$ are separated by an energy gap Δ from the gapless right-and left-moving states with $m = 0$, the latter gving rise to longitudinal dc conduction of nanotubes.

The field-driven redistribution of electrons reduces the value of the electric field inside the wire. This phenomenon, known as the depolarization effect, has first been addressed in the context of nanotubes in Ref. 3 and further studied in Refs. 4–6. Because of the limited number of transverse channels, the suppression is not complete. In the minimal electrostatic model, one can treat the wire as a solid cylinder with some effective dielectric permittivity $\varepsilon_\perp$. From elementary electrostatics [7] it then follows that the electric field inside the wire is uniform, $E_i = 2E_0/(1+\varepsilon_\perp)$, and reduced compared with the applied external field E_0. In terms of the effective transverse susceptibility $\alpha_\perp = (\varepsilon_\perp - 1)/4\pi$, this can be restated in the equivalent form,

$$E_i = \frac{E_0}{1+2\pi\alpha_\perp} = E_0\left[1 - 2\pi\alpha_\perp + (2\pi\alpha_\perp)^2 - ...\right]. \quad (1)$$

The meaning of the consecutive terms in this geometric series is rather transparent: the external field E_0 induces the surface charge density $\sigma = 2\pi\alpha_\perp E_0 \cos\theta$, where θ is the circumferential angle; this charge density produces the correction $E^{(1)} = -2\pi\alpha_\perp E_0$ to the field E_0. In turn, this correction induces additional charge density, and so on, resulting in the infinite series, Eq. (1).

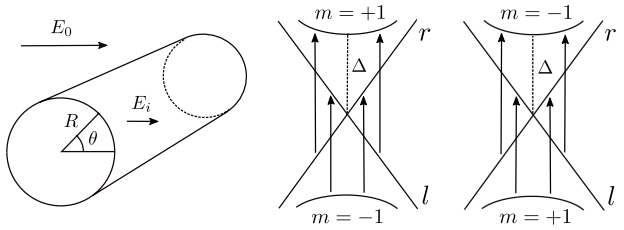

FIG. 1: Geometry of a nanutube in a transverse electric field (left) and the absorption transitions induced by such field: with the increase of the azimuthal angular momentum m, $0 \to +1$ and $-1 \to 0$ (center) and with the decrease of it, $0 \to -1$ and $+1 \to 0$ (right).

The same approach can be extended to an ac field [3, 4] as long as its frequency ω is low enough for the retardation to be disregarded: $\omega \ll c/R$, where R is the radius of the nanotube. Such condition is always satisfied for optical frequencies. Above the threshold frequency $\omega = \Delta$, the transitions between $m = 0$ and $m = \pm 1$ subbands become possible, Fig. 1. The imaginary part of $\alpha_\perp(\omega)$ determines the absorption spectrum. Calculating the amount of Joule heat generated per unit length of the tube, we can write it in either of the two equivalent forms,

$$Q = \frac{\pi}{2}\omega R^2 |E_i|^2 \alpha_\perp''(\omega) = \frac{\pi\omega}{2} R^2 |E_0|^2 \left(\frac{\alpha_\perp(\omega)}{1+2\pi\alpha_\perp(\omega)}\right)''. \quad (2)$$

It is our main finding that such intuitively appealing electrostatics approach nonetheless breaks down in the most interesting situation – near the absorption threshold, $\omega \approx \Delta$. Before explaining why it fails to account properly for the electron-electron Coulomb interaction, let us point out that Eqs. (1)-(2) are in fact equivalent to the Random Phase Approximation (RPA) [8]. In the latter, a system responds to a Fourier harmonic $\varphi_m(\omega)e^{im\theta}$ of a weak electric potential with the variation of the par-

ticle density,

$$\langle \rho_m(\omega)\rangle = \chi_m(\omega) e\varphi_m(\omega), \tag{3}$$

whose magnitude is determined by the polarization function

$$\chi_m(\omega) = -i\int\limits_0^\infty dt\ e^{i\omega t}\int\limits_{-\infty}^{\infty} dx\ \Big\langle\Big[\hat\rho_m(x,t),\hat\rho_{-m}(0,0)\Big]\Big\rangle, \tag{4}$$

which is a correlator of the electron density operators $\hat\rho_m(x,t)$ expressed as a sum over the channels with different azimuthal angular momenta: $\hat\rho_m(x,t) = \sum_\mu \hat\psi^\dagger_\mu(x,t)\hat\psi_{\mu+m}(x,t)$.

Because the potential, $\varphi = -RE_0(t)\cos\theta$, of a homogeneous external electric field E_0 contains only the dipolar Fourier harmonics, $\varphi_{\pm1} = -E_0R/2$, only the $m = \pm1$ components of the charge density can be excited. From symmetry it follows that $\langle\rho_1\rangle = \langle\rho_{-1}\rangle$. Utilizing Eq. (3) to relate the potential to the surface charge density, $\sigma = e\langle\rho_1\rangle\cos\theta/(\pi R)$, and then using the charge conservation law to find the sheet electric current flowing around the surface of the wire, one can calculate the amount of Joule heat dissipated in the wire,

$$Q = -\frac{\omega}{4}R^2e^2|E_0|^2\chi''(\omega). \tag{5}$$

(To ease notations, we omit the subscript 1 in $\chi_1(\omega)$.)

When Coulomb interaction is ignored, the correlation function (4) follows from the elementary Lindhard calculation [3] for the band structure of a nanotube, obtained by "rolling" a π-band of graphene [2]. At zero temperature, the only transitions with the change of the angular momentum +1 that are possible are those between the gapless right-movers $\epsilon = vp$ or left-movers $\epsilon = -vp$ subbands with $m = 0$ and the first gapped subbands $|\epsilon| = \sqrt{\Delta^2 + v^2p^2}$, where $\Delta = v/R$ is the energy gap; see Fig. 1. All four such processes contribute equally. For positive ω:

$$\begin{aligned}\chi^{(0)}(\omega) &= \frac{N}{\pi}\int\limits_0^\infty \frac{dp}{\omega - vp - \Delta - p^2/2m^* + i\eta}\\ &\approx \frac{N}{v\pi}\Big[\ln|\Omega| - i\pi\Theta(-\Omega)\Big], \quad \Omega = \frac{\Delta-\omega}{\Delta},\end{aligned} \tag{6}$$

Absorption can only occur if the frequency of the external field exceeds the gap, $\omega > \Delta$. In nanotubes, there are two orbital valleys and have two spin directions, so that the total electron flavor degeneracy $N = 4$.

Consider now the Coulomb interaction of electrons,

$$\hat V = \frac{1}{2}\sum_{\mu\nu m} V_m \int dx\, \hat\psi^\dagger_{\mu+m}(x)\hat\psi^\dagger_{\nu-m}(x)\hat\psi_\nu(x)\hat\psi_\mu(x), \tag{7}$$

with the matrix elements V_m for the scattering events that occur with the change of the angular momentum m previously found in Ref. 9. For non-zero m, $V_m = e^2/|m|$, while V_0 happens to be logarithmically stronger. For examle, $V_0 = 2e^2\ln(d/R)$, in a setting where a metallic gate is located some distance d away.

Coulomb interaction strongly modifies the absorption lineshape even though traditional exciton bound states [10] cannot be formed. Indeed, the absence of backscattering forbids velocity reversal of the gapless states. As a result, attractive Coulomb interaction between electrons and holes cannot confine them to a finite region of space.

Suppose first that one ignores V_0 and only retains $V_1 = e^2$ to account for the transverse polarization of the system. Because each closed electron loop brings the flavor degeneracy N, in the formal limit of $N \gg 1$ one can retain only the diagrams with the maximum possible number of the loops. This yields the RPA geometric series for the density-density correlation function (4), which consists of consecutive loops connected by the interactions V_1, as shown in Fig. 2,

$$RPA: \quad \chi(\omega) = \frac{\chi^{(0)}(\omega)}{1 - V_1\chi^{(0)}(\omega)}. \tag{8}$$

This expression together with Eq. (5) reproduces the dissipated power (2) as long as the transverse susceptibility is identified with the *non-interacting* ($V_0 = 0$) polarization operator: $\alpha_\perp(\omega) = -\frac{e^2}{2\pi}\chi^{(0)}(\omega)$. This result predicts that the threshold absorption at $\Omega = 0$, rather than being a step function, as in $\mathrm{Im}\chi^{(0)}(\omega)$, is suppressed as $\ln^{-2}\Omega$.

Ignoring V_0, however, can be problematic in one-dimensional systems [11–13]. For example, in nanotubes, the density of states of the gapless subbands has a power-law suppression, $\nu_0(\epsilon) \propto \epsilon^\alpha$ [14–17]. The exponent $\alpha = (1-g)^2/2Ng$ is customarily expressed via the effective coupling constant $g = v/u$, the ratio of the band velocity v and the velocity of the collective charged plasmon modes, $u = v\sqrt{1 + NV_0/\pi v}$. Similarly, the density of gapped states is suppressed as well, $\nu_1(\epsilon) \sim (\epsilon - \Delta)^{-1/2+\beta}$, compared with the non-interacting case [18]; the suppressing exponent is $\beta = (1-g^2)^2/2Ng$. These non-perturbative renormalizations originate from the decomposition of a single-electron state into an infinite number of charged plasmon modes [19].

The modification of the polarization function (6) by the V_0 interaction was studied in Ref. 20. In contrast to the density of states, the polarization function is *enhanced* at low Ω:

$$\chi^{(0)}_V(\omega) = -\frac{N\Gamma(\gamma)}{v\pi}\Big[\Omega^{-\gamma} - 1\Big], \quad \gamma = \frac{2 - g - g^3}{2N}, \tag{9}$$

with the subscript in $\chi^{(0)}_V$ indicating that the interaction V_0 is taken into account (the superscript reminding that one still assumes V_1=0). It is worth noting that the gapped state created in the interband transition acts similarly to a core-hole in the conventional X-ray edge singularity problem studied by Mahan [21] and Nozières

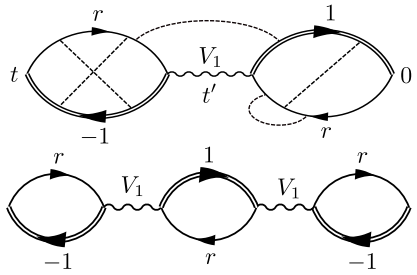

FIG. 2: First and second order corrections to the polarization function $\chi_1(\omega)$ in the interaction V_1 (wavy line). The interaction V_0 (dashed line) is accounted to all orders, including interactions between different loops (not shown in the second order diagram). The diagrams providing the leading contributions are shown. Massive gapped electrons $m = \pm 1$ are indicated with a double line; gapless states with a single line.

and De Dominicis [22]. The one notable difference is that in addition to the interaction with a core-hole, electrons themselves are strongly interacting. Nonetheless, the edge enhancement in Eq. (9) is the result of a competition between the Mahan-type enhancement and the Nozières-De Dominicis orthogonality catastrophe-type suppression for a given value of the interaction strength g.

The polarization function (9) determines the response of the nanotube to the actual electric field E_i inside it, $Q \propto -\mathrm{Im}\chi_V^{(0)}|E_i|^2 \propto \Omega^{-\gamma}|E_i|^2$, cf. the first identity in Eq. (2). However, to relate the inside field E_i to the applied field E_0 one also has to take into account the dipolar interaction V_1. It is the latter that is responsible for the redistribution of electrons around the circumference of the wire in response to a perpendicular electric field.

If one used the electrostatics/RPA mean-field approach embodied in Eqs. (2) and (8), one would arrive at the absorption, $Q \propto \Omega^{\gamma}|E_0|^2$, *suppressed* with the same exponent γ.

Below we show that the depolarization suppression of the near-threshold absorption is in fact much stronger,

$$Q \propto (\omega - \Delta)^{3\gamma}|E_0|^2, \tag{10}$$

and demonstrate that the conventional electrostatics fails because the independent-loop approximation does not apply in the presence of V_0-correlations between different loops, as illustrated in Fig. 2.

To account for the leading interaction V_0 to *all orders*, we use the bosonization approach [19] wherein the right- and left-moving gapless electronic operators are represented as the exponentials,

$$\hat{\psi}_{r,l}(t,x) = \frac{\hat{U}_{r,l}}{\sqrt{2\pi R}} e^{\hat{k}_{r,l}(t,x)}, \tag{11}$$

of the bosonic phases $\hat{k}_{r,l}$ with $\hat{U}_{r,l}$ being the fermionic counting operators. The inverse tube radius $1/R$ is chosen as the ultraviolet momentum cut-off. The bosonic phase operators are given by,

$$\hat{k}_{r,l}(t,x) = \sqrt{\pi}\sum_q \frac{1 \pm g\ \mathrm{sgn}\ q}{\sqrt{2gN|q|L}}\Big[\hat{a}_q e^{-i|q|ut+iqx} - c.c.\Big] + \sqrt{2\pi}\sum_{i=1}^{N-1}\sum_q \frac{\Theta(\pm q)}{\sqrt{N|q|L}}\Big[\hat{b}_{iq} e^{-i|q|vt+iqx} - c.c.\Big], \tag{12}$$

with the upper/lower signs corresponding to the right/left-moving electrons, respectively. The operators $\hat{a}_q$ represent the fast charged plasmon modes of the system, while the remaining $N-1$ modes $\hat{b}_{iq}$ are neutral (arising from the spin and band degeneracy) and propagating with the band velocity v; the Hamiltonian of the interacting gapless electrons is thus simply, $\hat{H} = u\sum_q |q|\hat{a}_q^\dagger\hat{a}_q + \sum_{i=1}^{N-1} v\sum_q |q|\hat{b}_{iq}^\dagger\hat{b}_{iq}$.

Although one cannot fully bosonize massive gapped states, it is possible to take advantage of the fact that for optical transitions near the threshold the momenta of the massive states are small and the electrons are virtually stationary there, $p/m \ll v, u$ [23]. Accordingly, massive states can be represented as a product [18, 20],

$$\hat{\psi}_1(t,x) = \hat{\psi}_1^{(0)}(t,x) e^{\hat{K}(t,x)}, \tag{13}$$

of a free fermion operator $\psi_1^{(0)}$ and the exponential of a phase, which is a time integral of the electric potential of the fluctuating plasmon field:

$$\hat{K}(t,x) = (1-g^2)\sum_q \sqrt{\frac{\pi}{2Ng|q|L}}\Big(\hat{a}_q e^{-i|q|ut+iqx} - c.c\Big). \tag{14}$$

Unlike the symmetric part of the interaction V_0, the dipolar interaction V_1 is not readily amenable to the bosonization technique. We are thus going to use a "hybrid" approach where V_1 is treated by means of the usual diagrammatic technique. For example, the main contribution to the first order in V_1 (shown in Fig. 2) turns out to be

$$\chi_V^{(1)}(\omega) \;=\; -\frac{V_1 N(N-1)}{4\pi^2 R^2}\int_0^\infty dt\ e^{i(\omega-\Delta)t}\int_0^t dt'\left\langle e^{-k_r(t)}e^{K(t)}e^{-2K(t')}e^{2k_r(t')}e^{K(0)}e^{-k_r(0)}\right\rangle, \tag{15}$$

where the averaging is performed over the Gaussian fluctuations of the bosonic fields. The integrals over the coordinates have already been eliminated from Eq. (15) owing to the sharply spatially localized propagators composed of the (slow) free fermion operators $\psi_1^{(0)}$. As a result, all the bosonic fields can be taken at $x = 0$ with only their time arguments shown in Eq. (15). The composition of the bosonic average in Eq. (15), as well as the signs of the operators in the exponents, can be traced to the nature and direction of the electron propagators shown in Fig. 2.

While the four different combinations of massive and massless propagators contribute *equally* to $\chi^{(1)}$ when V_0 is ignored, this is no longer the case for $V_0 \neq 0$. For example, the first order contribution is different where the electrons of the same chirality (left- or right-movers) propagate around both loops. The most singular contribution comes from the top diagram of Fig. 2, where both chiralities are the same and which yields the highest negative power, $\propto \Omega^{-3\gamma}$. Indeed, calculating the average in Eq. (15) and imposing a small-time cut-off $1/\Delta$ corresponding to high energies, we arrive at,

$$\chi^{(1)}(\omega) = \frac{V_1 N^2}{4\pi^2 v^2} \int\limits_{1/\Delta}^{\infty} \frac{dt}{t^\gamma}\, e^{i(\omega-\Delta)t} \int\limits_{1/\Delta}^{t-1/\Delta} \frac{dt'}{[(t-t')t']^{1-2\gamma}}$$
$$= \frac{V_1 N^2}{4\pi^2 v^2 \gamma^2} \Big[\frac{1}{3}\Big(\Omega^{-3\gamma} - 1\Big) - \Big(\Omega^{-\gamma} - 1\Big)\Big] \quad (16)$$

Here the integral is taken in the approximation of small γ, which is formally realized in the limit of a large number of channels $N \gg 1$. When $\gamma \ll 1$, it is the regions near the integration limits that contribute the most to the integrals.

The leading term in Eq. (16) has a greater power, $\Omega^{-3\gamma}$, than what could be naïvely expected ($\Omega^{-2\gamma}$) from a simple RPA product of the two loops each given by Eq. (9). Similarly, we identify the leading contributions to every order in V_1 as those that i) contain the same chirality (r or l) *in all loops* and ii) have two massive particles either created or destroyed at each V_1 interaction line. In the n-th order the leading contribution happens to be $\propto V_1^n \Omega^{-(2n+1)\gamma}$, which can be quickly established from power counting. The actual integrals for the numerical coefficients become very complicated in higher orders. However, it is possible to uniquely construct a series that obeys the following two properties: the n-th order term is an odd-power polynomial in $\Omega^{-\gamma}$, and the coefficients in the polynomial are chosen in such a way that in the limit of $\gamma \to 0$ the n-th order term reproduces $\ln^{n+1}\Omega$, the correct non-interacting ($V_0 = 0$) limit. This leads to the following expression

$$\chi_v^{(n)}(\omega) = -\frac{N}{\pi v} \frac{(-\lambda_1)^n}{\gamma^{n+1}} \sum_{j=0}^{n} A_j^{(n)} \Big(\Omega^{-(2j+1)\gamma} - 1\Big), \quad (17)$$

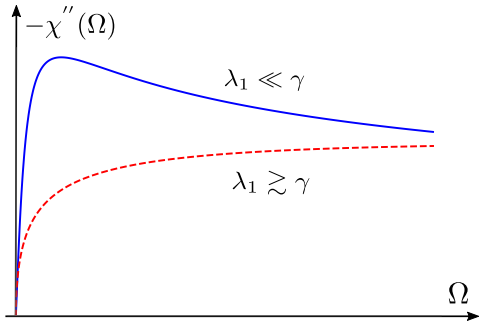

FIG. 3: [Color online] Absorption lineshape for different values of $V_1 = 4\pi v \lambda_1/N$. For small V_1 values (solid blue line) the suppression (depolarization) induced by it overcomes the enhancement due to V_0 sufficiently close to the threshold. For larger V_1 values the depolarization effect dominates everywhere.

where the effective dimensionless dipolar coupling constant is $\lambda_1 = NV_1/(4\pi v)$; the extra factor 1/4 originates from the fact that only one out of four possible loops has the strongest singularity at $\Omega = 0$.

The coefficients of the leading $j = n$ terms are $A_n^{(n)} = (n+1)/[2^n(2n+1)]$. The summation of these leading terms can be performed exactly with the identity,

$$\sum_{n=0}^{\infty} \frac{n+1}{n+\frac{1}{2}} y^{2n+1} = \frac{y}{1-y^2} + \operatorname{arctanh} y \approx \frac{i\pi}{2} - \frac{2}{3y^3}, \quad (18)$$

where the last approximation is valid for $y \gg 1$. Accordingly, we obtain that the imaginary part of the polarization operator close to the threshold is

$$\chi_v''(\omega) = -\frac{4N\gamma}{v\lambda_1^2} \left(\frac{\omega - \Delta}{\Delta}\right)^{3\gamma}. \quad (19)$$

The obtained result means that the optical absorption (5) close to the threshold $\omega = \Delta$ becomes suppressed due to the depolarization effect much more significantly than could be predicted based on the electrostatic mean field theory, $\propto (\omega - \Delta)^\gamma$. This can be viewed as a much stronger $E_i \propto (\omega - \Delta)^{2\gamma} E_0$ suppression of the electric field acting inside the wire, compared with Eq. (1).

The absorption lineshape is the result of an interplay between the symmetric V_0 and the dipolar V_1 interactions, see Fig. 3. The result (19) holds sufficiently close to the threshold no matter how small V_1 is: the latter is always relevant at $\Omega \to 0$. The magnitude of V_1 determines how close to the threshold the transition to the domain of Eq. (19) happens. If $\lambda_1 \ll \gamma$, the interaction V_1 is not important far from the threshold, where the absorption is given by the imaginary part of Eq. (9), $\chi_v'' = -N\Omega^{-\gamma}/v$, which increases with decreasing Ω. At $\Omega^{2\gamma} \sim \lambda_1/\gamma$ the frequency dependence of the absorption crosses over to that of Eq. (19) and drops sharply at the threshold. If, in contrast, the interaction V_1 is not

very small, so that $\lambda_1 \gtrsim \gamma$, the expression (19) should be used everywhere near the threshold. This is what is expected to happen in metallic carbon nanotubes. The absorption given by Eqs. (5) and (19) should be testable in optical absorption measurements. Even though previous measurements of transverse absorption [24, 25] do not provide sufficient resolution near the threshold, the modern advances in nanotube manufacturing [26] should make such measurement possible.

Finally, we note that although the depolarization effect exists in both semiconducting and metallic nanotubes, the physical mechanisms implicated in the two cases are different. As shown above, depolarization effect in metallic nanotubes is dominated by the shake-up of an infinite number of low-lying plasmon excitations. In contrast, in semiconducting nanotubes with no gapless states, where conventional excitonic effects can be expected to dominate, various *ab initio* approaches, such as the Bethe-Salpeter method, should be used [27, 28].

Discussions with O. Starykh, S. LeBohec, and D. Pesin are gratefully acknowledged. This work was supported by DOE, Office of Basic Energy Sciences, Grant No. DE-FG02-06ER46313.

[1] V. V. Deshpande, M. Bockrath, L. I. Glazman, A. Yacoby, Nature **464**, 209 (2010).
[2] R. Saito, G. Dresselhaus, and M. S. Dresselhaus, *Physical Properties of Carbon Nanotubes* (Imperial College Press, London, 1998).
[3] H. Ajiki and T. Ando, Physica (Amsterdam) **201B**, 349 (1994).
[4] L. X. Benedict, S. G. Louie, and M. L. Cohen, Phys. Rev. B **52**, 8541 (1995).
[5] S. Tasaki, K. Maekawa, and T. Yamabe, Phys. Rev. B **57**, 9301 (1998).
[6] A. G. Marinopoulos, L. Reining, A. Rubio, and N. Vast, Phys. Rev. Lett. **91**, 046402 (2003).
[7] L. D. Landau and E. M. Lifshitz, *Electrodynamics of Continuous Media* (Pergamon Press, London, 1960).
[8] G. Mahan, *Many-Particle Physics*, (Plenum Press, New York, 1990).
[9] E. G. Mishchenko, A.V. Andreev, and L. I. Glazman, Phys. Rev. Lett. **87**, 246801 (2001).
[10] T. Ando, T. Nakanishi, and R. Saito, J. Phys. Soc. Jpn. **67**, 2857 (1998).
[11] D. C. Mattis and E. H. Lieb, J. Math. Phys. **6**, 304 (1965).
[12] I. E. Dzyaloshinskii and A. I. Larkin, Sov. Phys. JETP **38**, 202 (1974).
[13] F. D. M. Haldane, J. Phys. C **14**, 2585 (1981).
[14] C. L. Kane, L. Balents and M. P. A. Fisher, Phys. Rev. Lett. **79**, 5086 (1997); R. Egger and A. O. Gogolin, Phys. Rev. Lett. **79**, 5082 (1997).
[15] M. Bockrath, D. H. Cobden, J. G. Lu, A. G. Rinzler, R. E. Smalley, L. Balents, and P. L. McEuen, Nature **397**, 598 (1999).
[16] Z. Yao, H. W. Ch. Postma, L. Balents, C. Dekker, Nature **402**, 273 (1999).
[17] H. Ishii, H. Kataura, H. Shiozawa, H. Yoshioka, H. Otsubo, Y. Takayama, T. Miyahara, S. Suzuki, Y. Achiba, M. Nakatake, T. Narimura, M. Higashiguchi, K. Shimada, H. Namatame and M. Taniguchi, Nature **426**, 540 (2003).
[18] L. Balents, Phys. Rev. B **61**, 4429 (2000).
[19] T. Giamarchi, *Quantum Physics in One Dimension* (Clarendon Press, Oxford, 2004).
[20] E. G. Mishchenko and O. A. Starykh, Phys. Rev. Lett. **107**, 116804 (2011).
[21] G. D. Mahan, Phys. Rev. **163**, 612 (1967).
[22] P. Nozires and C. T. De Dominicis, Phys. Rev. **178**, 1097 (1969).
[23] Heavy slow particles invoke edge singularity "core-hole" physics, which in relation to quantum wires was first discussed by T. Ogawa, A. Furusaki, and N. Nagaosa, Phys. Rev. Lett. **68**, 3638 (1992).
[24] W. Z. Liang, G. H. Chen, Z. Li, and Z. K. Tang, Appl. Phys. Lett. **80**, 3415 (2002).
[25] Z. M. Li, Z. K. Tang, H. J. Liu, N. Wang, C. T. Chan, R. Saito, S. Okada, G. D. Li, J. S. Chen, N. Nagasawa, and S. Tsuda, Phys. Rev. Lett. **87**, 127401 (2001).
[26] E. H. Hároz, J. G. Duque, X. Tu, M. Zheng, A. R. Hight Walker, R. H. Hauge, S. K. Doorn and J. Kono, Nanoscale **5**, 1411 (2013).
[27] C. D. Spataru, S. Ismail-Beigi, L. X. Benedict, and S. G. Louie, Phys. Rev. Lett. **92**, 077402 (2004).
[28] L. X. Benedict, Phys. Rev. B **66**, 193105 (2002)